IEEE Access
Multidisciplinary | Rapid Review | Open Access Journal

Received June 2, 2020, accepted June 8, 2020, date of publication June 23, 2020, date of current version July 7, 2020.

*Digital Object Identifier 10.1109/ACCESS.2020.3004456*

# A Robust State Estimation Method for Unknown, Time-Varying and Featureless Aircraft Sensor Failures

**HONGBO WANG[1], (Member, IEEE), DONG LIU[2], TIANYU CHEN[3], AND XIANSHENG QIN[1], (Member, IEEE)**

[1]School of Mechanical Engineering, Northwestern Polytechnical University, Xi'an 710072, China
[2]First Aircraft Institute, Aviation Industry Corporation of China, Xi'an 710089, China
[3]School of Electronic Engineering, Xi'an University of Posts and Telecommunications, Xi'an 710121, China

Corresponding author: Dong Liu (ldleo@sina.com)

This work was supported by NSFC under Grant 61603298.

**ABSTRACT** Fault-tolerant state estimation is necessary for analytical redundancy in aviation safety, but complicated fault conditions pose a major challenge to reliable estimations. In this paper, we propose a new state-estimation method based on an intermittent-measurement Kalman filter, a maximum-likelihood estimation rule, and the Gaussian mixture reduction. This method is robust to time-varying and featureless faults, and requires no past history of innovation errors to perform fault detection and isolation, leading to the easy implementation and improved accuracy under severe sensor-failure conditions. With an example application of monitoring the rotation speeds of a two-spool jet engine in simulations, the effectiveness of the proposed method is verified.

**INDEX TERMS** State estimation, intermittent measurements, fault detection, Kalman filter, jet engine.

## NOMENCLATURE

| | |
|---|---|
| Bold, upper case symbols: | Matrices |
| Bold, lower case symbols: | Vectors |
| Symbols with hat: | Estimated variables |
| Symbols with tilde: | Variables perturbed by noises and faults |
| Right superscript $(j)$: | Variables under fault condition $j$ |
| Right subscript $k\lfloor j$: | Variables inferred at moment $k$, using the information from moment $j$ |
| $\boldsymbol{A_d}$ | State matrix of the discrete linear system in (1) |
| $\boldsymbol{B_d}$ | Input matrix of the discrete linear system in (1) |
| $\boldsymbol{c}_i^T$ | The $i$th row of $\boldsymbol{C_d}$ |
| $\boldsymbol{C_d}$ | Output matrix of the discrete linear system in (1) |
| $\boldsymbol{G}_j$ | The selection matrix excluding the all-zero rows of diag$(\boldsymbol{\gamma}^{(j)})$ |
| $\boldsymbol{K}_k^{(j)}$ | The Kalman gain at moment $k$ and under fault condition $\boldsymbol{\gamma}^{(j)}$ |
| $\boldsymbol{P}_{k\|k}^{(j)}$ | The corrected covariance matrix of estimation error at moment $k$ and under fault condition $\boldsymbol{\gamma}^{(j)}$ |
| $\boldsymbol{P}_{k\|k-1}$ | Predicted covariance matrix of estimation error for moment $k$, using information from moment $k-1$ |
| $\boldsymbol{P}_{k\|k}$ | Corrected covariance matrix of estimation error at moment $k$ |
| $\boldsymbol{Q}$ | Covariance matrix of process noise |
| $\boldsymbol{R}$ | Covariance matrix of measurement noise |
| $\boldsymbol{S}_k^{(j)}$ | Covariance matrix of the innovation error in (10) |
| $\boldsymbol{T}_1$,$\boldsymbol{T}_2$ | Intermediate-variable matrices given in (18) |
| $\boldsymbol{u}_k$ | Input vector at moment $k$ |
| $\boldsymbol{v}_k$ | Measurement noise at moment $k$ |
| $\boldsymbol{w}_k$ | Process noise at moment $k$ |
| $\boldsymbol{x}_k$ | System state vector at moment $k$ |

The associate editor coordinating the review of this manuscript and approving it for publication was Yanbo Chen.

| | |
|---|---|
| $\boldsymbol{y}_k$ | Measurement vector at moment $k$ |
| $\mathcal{N}(\boldsymbol{a}, \boldsymbol{B})$ | Gaussian probability density function with mean $\boldsymbol{a}$ and covariance $\boldsymbol{B}$ |
| $P(\boldsymbol{\gamma}^{(j)})$ | Probability of the fault condition $\boldsymbol{\gamma}^{(j)}$ in (13) |
| $\hat{\boldsymbol{x}}_{k\|k}^{(j)}$ | Corrected estimation at moment $k$ and under fault condition $\boldsymbol{\gamma}^{(j)}$ |
| $\hat{\boldsymbol{x}}_{k\|k-1}$ | Predicted estimation for moment $k$, using information from moment $k-1$ |
| $\hat{\boldsymbol{x}}_{k\|k}$ | Corrected estimation at moment $k$ |
| $\tilde{\boldsymbol{C}}_k^{(j)}$ | Modified output matrix at moment $k$ and under fault condition $\boldsymbol{\gamma}^{(j)}$, in (7) |
| $\tilde{\boldsymbol{M}}_k^{(j)}$ | Covariance correction term at moment $k$ and under fault condition $\boldsymbol{\gamma}^{(j)}$, in (7) |
| $\tilde{\boldsymbol{R}}_k^{\dagger}$ | The left pseudoinverse of matrix $\tilde{\boldsymbol{R}}_k$ |
| $\tilde{\boldsymbol{R}}_k^{(j)}$ | Modified covariance matrix of measurement noises, at moment $k$ and under fault condition $\boldsymbol{\gamma}^{(j)}$, in (7) |
| $\tilde{\boldsymbol{y}}_k$ | Real measurement vector under noises and sensor faults at moment $k$ |
| $a_{95\%}$ | Area of the 95%-confidence ellipse for an error distribution |
| $m$ | Dimension of the measurement vector $\boldsymbol{y}$ |
| $n$ | Dimension of the system state vector $\boldsymbol{x}$ |
| $r_i$ | The $i$th-row, $i$th-column entry of matrix $\boldsymbol{R}$ |
| $z_{\text{stop}}$ | The iteration stop condition in Algorithm 1 |
| $\boldsymbol{\epsilon}_k^{(j)}$ | Innovation error under fault condition $\boldsymbol{\gamma}^{(j)}$ in (9) |
| $\boldsymbol{\Gamma}$ | Matrix containing the set of all possible fault conditions in (5) |
| $\boldsymbol{\gamma}_k$ | Fault-condition vector at moment $k$ in (2) |
| $\boldsymbol{\gamma}^{(j)}$ | The $m$-dimensional binary representation of integer $j$ in (6) |
| $\boldsymbol{\lambda}$ | Vector of fault-free probabilities in (3) |
| $\delta_{\text{exp}}$ | The expected standard deviation percentage in (20) |
| $\gamma_{k,i}$ | The $i$th component of $\boldsymbol{\gamma}_k$ |
| $\xi^{(j)}$ | The conditional probability of $\boldsymbol{\gamma}^{(j)}$ in (14) |
| $\bar{\Delta}$ | The state-variation threshold in Algorithm 1 |

## I. INTRODUCTION

Reliable sensor feedbacks are essential to aviation safety. To protect aircrafts from sensor failures, hardware redundancy, which uses duplicated and independent sensor pathways, has been widely implemented, e.g., in flight control systems [1]. However, due to cost and weight restrictions, it is impractical to apply hardware redundancy to all subsystems of aircrafts, and many ''non-critical'' sensor pathways have no redundancy. One example is the spool-speed feedback path, from the jet engine controller to the human–machine interface (EWD), via the engine interface unit (EIU) [2] (illustrated as the arrow-connected blocks in the bottom of Fig. 1)—Though a failure in the path does not affect the self-contained engine control system [3], incorrect engine-speed readings in the EWD mislead pilots and may result in severe safety problems.

To increase system robustness without relying on hardware redundancies, Patton proposed the use of *analytical redundancy*, i.e., combining the model knowledge and dissimilar sensors' measurements, for increasing the robustness of sensor systems [4], [5]. For the exemplified application shown in Fig. 1, the analytical redundancy can be formed by combining the jet engine's nominal model with various sensors' measurements, such as the LPC/HPC (low/high-pressure compressor) speeds, generator input-shaft speed, bleed pressure/flow rate, and total air pressure/temperature data. Due to measurements noises and unknown faults in the sensor pathways, many investigations have been conducted on two necessary components of analytical redundancy, namely the fault detection and isolation (FDI), and the state estimation methods.

On FDI, a key indicator of sensor fault is the *innovation error*, which is defined as the difference between the expected and real sensor measurements. For example, the sum of squared innovation errors for multiple fault assumptions are compared to find the true fault condition [6]–[10]. Normality tests are performed on past innovation errors within a moving window to detect a fault [11], [12]. Threshold tests on the innovation errors have also been implemented [5], [13].

On state estimation, the classic Kalman filter (KF) and its nonlinear extensions, particularly the unscented Kalman filter (UKF) [14], have been widely implemented and tailored for estimating system state under fault conditions. For example, the multiple model adaptive estimation (MMAE) methods use multiple parallel classic KFs [6]–[10]. The adaptive-KF methods, such as the innovation/residual-based adaptive estimation (IAE/RAE) [15]–[18] and the robust adaptive KF (RAKF) [11], [12], improve classic KF by introducing adaptive covariance matrices of process and measurement noises. This adaption technique has also been extended to UKFs [13].

The above methods have been successfully implemented in applications demanding fault-tolerant state estimations. But we still have the following problems if the measurement situations are severe, for example:

- Hardware failures may either be permanent or temporary, depending on the diversified fault types from hardware destructions to poor electrical contacts, hence the fault conditions can be time-varying;
- Faults may occur at different locations in the sensor pathways, from the variable-resistance sensors to the power supply chips, etc. Accordingly, the outputs of faulty paths may not have specific features in either time or frequency domains.

Due to the above situations, the following difficulties may be encountered:

- For FDI, the assumption on constant fault condition, which is the basis for comparing multiple series of recorded innovations errors, does not hold. Moreover, normality tests on the innovation errors are sensitive to the successful removal of faulty measurements inside

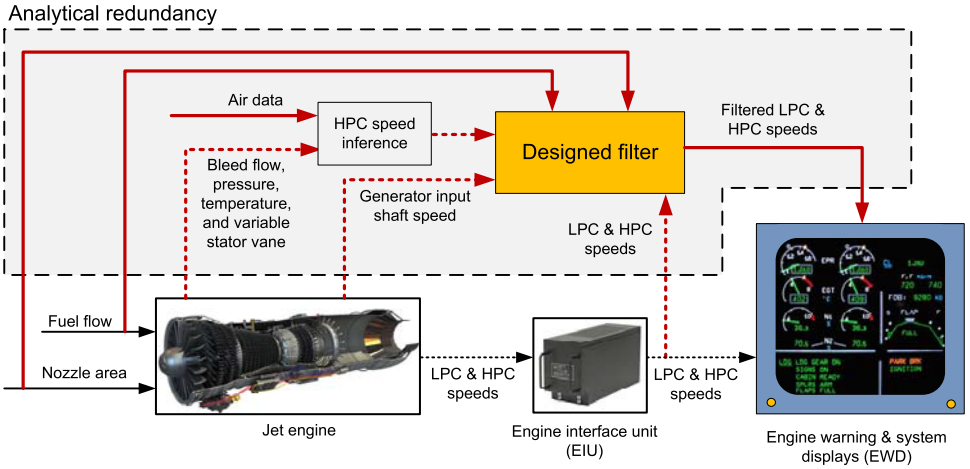


**FIGURE 1.** Overview of the system for monitoring the LPC and HPC speeds. Dashed arrows indicate the non-redundant sensor pathways subject to potential failures.

a time window, which is a challenging job under the time-varying faults and featureless outputs. Besides, the threshold-based FDI methods demand much tuning work to fit specific applications.

- The adaptive KF/UKF is dependent on the past innovation errors, the introduced lag results in performance sacrifice. Furthermore, the convergence of the adaptive KF is based on the linear time-invariant (LTI) stability condition [15], which may not hold under rapidly time-varying faults.

In this paper, based on an intermittent-measurement KF (IMKF) [19], [20], a maximum-likelihood estimation rule, and the Gaussian mixture reduction, we propose a new state-estimation method that has the following improvements over the classic methods:

- Time-varying intermittent faults can be handled properly without relying on the LTI assumption (the basis of adaptive-type methods) [15], leading to expanded application scenarios;
- Unlike the IMKF discussed in [19], [20] for intermittent communications, where data-missing faults are explicit, the proposed method allows the introduction of unknown faults, and made no assumption on the faulty signals' patterns. This corresponds to a more realistic situation in practice;
- The FDI is independent of the past history of innovation errors, avoiding the possible lags that may sacrifice performance. Besides, the FDI needs no user-specified parameters. This reduces the risks in tuning/testing, and allows the easy-implementation of the proposed method.

The rest of this paper is organized as follows: The state-estimation problem under sensor faults is introduced in Section II. The general idea and the details of the proposed method are presented in Section III. As a case study, the proposed method is applied to the spool-speed monitor application (Fig. 1), and its performance is compared with those of the other classic methods in Section IV. Conclusions are given in Section V.

## II. PROBLEM FORMULATION

For the system to be monitored, we assume that its dynamics can be described by a linear discrete model.[1] Let $\boldsymbol{x}_k \in \mathbb{R}^n$ be the system state at moment $k$, $\boldsymbol{u}_k \in \mathbb{R}^r$ be the input vector, and $\boldsymbol{y}_k \in \mathbb{R}^m$ be the sensors' outputs under the fault-free condition, the system dynamics is given by:

$$\begin{aligned} \boldsymbol{x}_{k+1} &= \boldsymbol{A_d}\boldsymbol{x}_k + \boldsymbol{B_d}\boldsymbol{u}_k + \boldsymbol{w}_k, \\ \boldsymbol{y}_k &= \boldsymbol{C_d}\boldsymbol{x}_k + \boldsymbol{v}_k, \end{aligned} \tag{1}$$

where $\boldsymbol{A_d}$, $\boldsymbol{B_d}$, and $\boldsymbol{C_d}$ are matrices describing the linear system, $\boldsymbol{w}_k \in \mathbb{R}^n$ is the process noises, and $\boldsymbol{v}_k \in \mathbb{R}^m$ denotes the sensors' noises. $\boldsymbol{w}_k$ and $\boldsymbol{v}_k$ are assumed to be independent, zero-mean, and Gaussian, with diagonal covariance matrices given by $\boldsymbol{Q}$ and $\boldsymbol{R}$, respectively.

To describe the fault condition at moment $k$, a binary vector is introduced as

$$\boldsymbol{\gamma}_k = [\gamma_{k,1}, \gamma_{k,2}, \ldots, \gamma_{k,m}]^T, \tag{2}$$

where $\gamma_{k,i} = 1$ indicates that the $i$th component of $\boldsymbol{y}_k$ is fault-free, and $\gamma_{k,i} = 0$ means that the component is malfunctioned.

Besides, a vector of fault-free probabilities is given by

$$\boldsymbol{\lambda} = [\lambda_1, \lambda_2, \ldots, \lambda_m]^T, \tag{3}$$

where $\lambda_i$ is the expected fault-free probabilities of the $i$th sensor path, i.e, $\lambda_i = \boldsymbol{E}(\gamma_{k,i})$. To characterize the fault behaviors, the following assumptions are made:

1) Faults can either be intermittent or permanent, corresponding to occasions like bad electrical contacts, poorly shielded data buses, and hardware damages, etc.;
2) The fault-condition vector $\boldsymbol{\gamma}_k$ at moment $k$ is unknown, and the fault-free probability vector $\boldsymbol{\lambda}$ is only roughly known, which is a common situation in practice;

[1] Although jet engines' dynamics are intrinsically nonlinear, the linearized models have been successfully and widely used in engine controls [21].

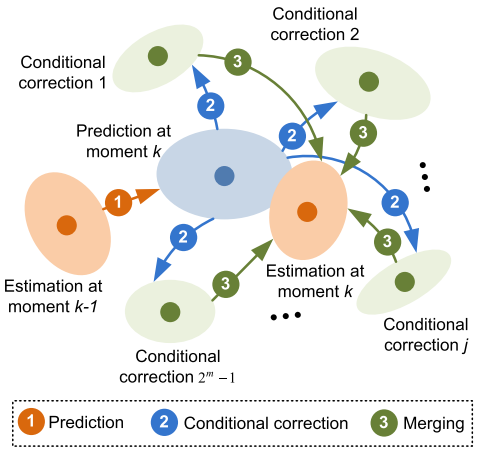


**FIGURE 2.** Illustration of the estimation process.

3) When a sensor path is malfunctioned, its output is featureless and could have any value.

Let $\tilde{\boldsymbol{y}}_1, \tilde{\boldsymbol{y}}_2, \ldots, \tilde{\boldsymbol{y}}_k$ be the measurements subject to sensor faults satisfying the above assumptions, our goal is to estimate the system state and covariance at moment $k$ with the proposed method, which is discussed in the subsequent section.

## III. PROPOSED METHOD

The general idea of the proposed method is illustrated in Fig. 2, showing how the $k$th estimation is obtained from the $(k-1)$th result. As shown in Fig. 2, the estimation process includes the following three stages:

1) Prediction: Predicting the state and covariance for moment $k$ using the model knowledge and previous estimation results;
2) Conditional correction: For each possible fault condition, correcting the prediction using the measurements at moment $k$;
3) Merging: By merging the multiple results of conditional corrections, arriving at the estimation results at moment $k$.

The above stages are detailed blow:

### A. PREDICTION

Let the $\hat{\boldsymbol{x}}_{k-1|k-1}$ and $\boldsymbol{P}_{k-1|k-1}$ be the state estimation and covariance at moment $k-1$, respectively. The prediction at moment $k$ is obtained using the the model knowledge:

$$\begin{aligned}\hat{\boldsymbol{x}}_{k|k-1} &= \boldsymbol{A_d}\hat{\boldsymbol{x}}_{k-1|k-1} + \boldsymbol{B_d}\boldsymbol{u}_{k-1},\\ \boldsymbol{P}_{k|k-1} &= \boldsymbol{A_d}\boldsymbol{P}_{k-1|k-1}\boldsymbol{A_d}^T + \boldsymbol{Q},\end{aligned} \tag{4}$$

where $\hat{\boldsymbol{x}}_{k|k-1}$ and $\boldsymbol{P}_{k|k-1}$ are the predicted state and covariance, respectively.

### B. CONDITIONAL CORRECTION

In this stage, $\hat{\boldsymbol{x}}_{k|k-1}$ and $\boldsymbol{P}_{k|k-1}$ are to be corrected using the faulty measurements $\tilde{\boldsymbol{y}}_k$. Unlike the classic KF, this correction stage is dependent on the sensors' fault conditions. Let $\boldsymbol{\Gamma}$ be the set of all possible fault conditions:

$$\boldsymbol{\Gamma} = \left\{\boldsymbol{\gamma}^{(1)}, \boldsymbol{\gamma}^{(2)}, \ldots, \boldsymbol{\gamma}^{(2^m-1)}\right\}, \tag{5}$$

where $\boldsymbol{\gamma}^{(j)}$ denotes the $m$-dimensional binary representation of $j$, i.e.,

$$\begin{aligned}\boldsymbol{\gamma}^{(1)} &= [0, 0, \ldots, 0, 0, 1]^T,\\ \boldsymbol{\gamma}^{(2)} &= [0, 0, \ldots, 0, 1, 0]^T,\\ &\vdots\\ \boldsymbol{\gamma}^{(2^m-1)} &= [1, 1, \ldots, 1, 1, 1]^T.\end{aligned} \tag{6}$$

For the $j$th fault condition $\boldsymbol{\gamma}^{(j)}$, three matrices for the conditional correction are defined in the IMKF [20] as

$$\begin{aligned}\tilde{\boldsymbol{C}}_k^{(j)} &= \mathrm{diag}(\boldsymbol{\gamma}^{(j)})\boldsymbol{C_d},\\ \tilde{\boldsymbol{R}}_k^{(j)} &= \mathrm{diag}(\boldsymbol{\gamma}^{(j)})\boldsymbol{R},\\ \tilde{\boldsymbol{M}}_k^{(j)} &= \sum_{i=1}^{m}\frac{\gamma_{k,i}}{r_i}\boldsymbol{c}_i\boldsymbol{c}_i^T,\end{aligned} \tag{7}$$

where $r_i$ is the $i$th-row, $i$th-column entry of $\boldsymbol{R}$ (covariance of measurement noise), and $\boldsymbol{c}_i^T$ is the $i$th row of $\boldsymbol{C_d}$ in (1). Then the conditional correction under fault condition $\boldsymbol{\gamma}^{(j)}$ is given by [20]:

$$\begin{aligned}\boldsymbol{P}_{k|k}^{(j)} &= \left(\boldsymbol{P}_{k|k-1}^{-1} + \tilde{\boldsymbol{M}}_k\right)^{-1},\\ \boldsymbol{K}_k^{(j)} &= \boldsymbol{P}_{k|k}^{(j)}\tilde{\boldsymbol{C}}_k^T\tilde{\boldsymbol{R}}_k^{\dagger},\\ \hat{\boldsymbol{x}}_{k|k}^{(j)} &= \hat{\boldsymbol{x}}_{k|k-1} + \boldsymbol{K}_k^{(j)}\left(\tilde{\boldsymbol{y}}_k - \tilde{\boldsymbol{C}}_k^{(j)}\hat{\boldsymbol{x}}_{k|k-1}\right),\end{aligned} \tag{8}$$

where $\boldsymbol{K}_k^{(j)}$ is the Kalman gain, and $(\cdot)^{\dagger}$ denotes the left pseudoinverse of a matrix.

### C. MERGING

To compute innovation errors, the faulty sensors' channels must be removed. To do that, we introduce a "selection matrix" $\boldsymbol{G}_j$, which excludes the all-zero rows of $\mathrm{diag}(\boldsymbol{\gamma}^{(j)})$. Thus the innovation error under fault condition $\boldsymbol{\gamma}^{(j)}$ is given by

$$\boldsymbol{\varepsilon}_k^{(j)} = \boldsymbol{G}_j\tilde{\boldsymbol{y}}_k - \boldsymbol{G}_j\boldsymbol{C_d}\hat{\boldsymbol{x}}_{k|k-1}. \tag{9}$$

The covariance of the innovation error under $\boldsymbol{\gamma}^{(j)}$ is

$$\boldsymbol{S}_k^{(j)} = \boldsymbol{G}_j\boldsymbol{C_d}\boldsymbol{P}_{k|k-1}\boldsymbol{C_d}^T\boldsymbol{G}_j^T + \boldsymbol{G}_j\tilde{\boldsymbol{R}}_k^{(j)}\boldsymbol{G}_j^T. \tag{10}$$

Then the probability density function of $\boldsymbol{\varepsilon}_k^{(j)}$ under fault condition $\boldsymbol{\gamma}^{(j)}$ is:

$$p(\boldsymbol{\varepsilon}_k^{(j)}|\boldsymbol{\gamma}^{(j)}) = p\left(\boldsymbol{\varepsilon}_k^{(j)}|\mathcal{N}(\boldsymbol{0}, \boldsymbol{S}_k^{(j)})\right), \tag{11}$$

where $\mathcal{N}(\boldsymbol{0}, \boldsymbol{S}_k^{(j)})$ denotes the Gaussian probability density function with mean $\boldsymbol{0}$ and covariance $\boldsymbol{S}_k^{(j)}$.

Let $l_i$ be the probability of the $i$th sensor's current fault condition, i.e.,

$$l_i = \begin{cases}\lambda_i, & \gamma_i^{(j)} = 1,\\ 1-\lambda_i, & \gamma_i^{(j)} = 0,\end{cases} \tag{12}$$

where $\gamma_i^{(j)}$ is the $i$th element of $\boldsymbol{\gamma}^{(j)}$. Then the probability of the fault condition $\boldsymbol{\gamma}^{(j)}$, denoted by $P(\boldsymbol{\gamma}^{(j)})$, is given by

$$P(\boldsymbol{\gamma}^{(j)}) = \prod_{i=1}^{m} l_i. \tag{13}$$

With the above formulations, we can now compute the merging weights $\xi^{(j)}$, which is the conditional probability of $\boldsymbol{\gamma}^{(j)}$ under the observed innovation error $\boldsymbol{\varepsilon}_k^{(j)}$. This condition probability can be obtained by the continuous Bayes equation:

$$\begin{aligned}\xi^{(j)} &\triangleq P(\boldsymbol{\gamma}^{(j)}|\boldsymbol{\varepsilon}_k^{(j)}) \\ &= \frac{p(\boldsymbol{\varepsilon}_k^{(j)}|\boldsymbol{\gamma}^{(j)})P(\boldsymbol{\gamma}^{(j)})}{\sum_{i=1}^{2^m-1}\left(p(\boldsymbol{\varepsilon}_k^{(i)}|\boldsymbol{\gamma}^{(i)})P(\boldsymbol{\gamma}^{(i)})\right)},\end{aligned} \tag{14}$$

where $p(\boldsymbol{\varepsilon}_k^{(j)}|\boldsymbol{\gamma}^{(j)})$ has been given in (11), and $P(\boldsymbol{\gamma}^{(j)})$ is in (13).

By performing Gaussian mixture reduction [22], the conditional corrections under all fault conditions are merged with weights $\xi^{(1)}, \xi^{(2)}, \ldots, \xi^{(2^m-1)}$:

$$\hat{\boldsymbol{x}}_{k|k} = \sum_{j=1}^{2^m-1}\left(\xi^{(j)}\hat{\boldsymbol{x}}_{k|k}^{(j)}\right), \tag{15}$$

$$\boldsymbol{P}_{k|k} = \boldsymbol{T}_1 + \boldsymbol{T}_2, \tag{16}$$

where

$$\boldsymbol{T}_1 = \sum_{j=1}^{2^m-1}\left(\xi^{(j)}\boldsymbol{P}_{k|k}^{(j)}\right), \tag{17}$$

$$\boldsymbol{T}_2 = \sum_{j=1}^{2^m-1}\left(\xi^{(j)}\left(\hat{\boldsymbol{x}}_{k|k}^{(j)} - \hat{\boldsymbol{x}}_{k|k}\right)\left(\hat{\boldsymbol{x}}_{k|k}^{(j)} - \hat{\boldsymbol{x}}_{k|k}\right)^T\right). \tag{18}$$

Furthermore, the following steps are also needed for a complete estimation method:

1) Determining the initial estimation $\hat{\boldsymbol{x}}_{0|0}$ and covariance $\boldsymbol{P}_{0|0}$;
2) Specifying a stop condition for entering and exiting the iterative estimation process;
3) Thresholding $\hat{\boldsymbol{x}}_{k|k} - \hat{\boldsymbol{x}}_{k-1|k-1}$ with a maximum variation-rate limit to avoid rare cases where all sensors fail simultaneously;
4) Determining the process-noise-covariance $\boldsymbol{Q}$ and measurement noise covariance $\boldsymbol{R}$ from pilot experiment data and least-squares fitting [23].

Finally, the proposed method is summarized in Algorithm 1. While Kalman-type filters has polynomial complexity with respect to (w.r.t.) the system's state dimension $n$, the number of conditional corrections (i.e., line 6–19 in Algorithm 1) grows exponentially w.r.t the output dimension $m$. Though expensive, this exponential complexity are alleviated by the following two facts:

- In aircrafts, due to weight and reliability constraints, sensors related with a specific subsystem is usually limited in number; this avoids the situation of large $m$;
- For different fault conditions, the conditional corrections are independent with each other, as they share no common variables/resources. Therefore, for those applications with large $m$, the conditional correction stage can be fully parallelized to speedup the computations.

**Algorithm 1** The Proposed State-Estimation Method

**Input**: System model $\boldsymbol{A_d}, \boldsymbol{B_d}, \boldsymbol{C_d}$, process noise covariance $\boldsymbol{Q}$, sensor output noise covariance $\boldsymbol{R}$, fault-condition set $\boldsymbol{\Gamma}$, fault-free probabilities $\boldsymbol{\lambda}$, inputs $\boldsymbol{u}_1, \boldsymbol{u}_2, \boldsymbol{u}_3, \ldots$, etc., measurements $\tilde{\boldsymbol{y}}_1, \tilde{\boldsymbol{y}}_2, \tilde{\boldsymbol{y}}_3, \ldots$, etc., state-variation threshold $\bar{\Delta}$, and iteration stop condition $z_{\text{stop}}$.

**Output**: State estimations $\hat{\boldsymbol{x}}_{1|1}, \hat{\boldsymbol{x}}_{2|2}, \hat{\boldsymbol{x}}_{3|3}, \ldots$, etc., and estimation covariances $\boldsymbol{P}_{1|1}, \boldsymbol{P}_{2|2}, \boldsymbol{P}_{3|3}, \ldots$, etc.

1 Initialization: $k \leftarrow 0$, set the initial state estimation $\hat{\boldsymbol{x}}_{0|0}$ and covariance $\boldsymbol{P}_{0|0}$;
2 **while** $z_{stop} \neq$ `true` **do**
3  $k \leftarrow k + 1$;
4  Predict $\hat{\boldsymbol{x}}_{k|k-1}$ and $\boldsymbol{P}_{k|k-1}$ using (4);
5  `den` $\leftarrow 0$;
6  **for** $j = 1$ **to** $2^m - 1$ **do**
7  Obtain the conditional correction $\hat{\boldsymbol{x}}_{k|k}^{(j)}$ and $\boldsymbol{P}_{k|k}^{(j)}$ with (7) and (8);
8  Compute the innovation error $\boldsymbol{\varepsilon}_k^{(j)}$ and its covariance $\boldsymbol{S}_k^{(j)}$ with (9) and (10);
9  Compute the conditional probability density $p(\boldsymbol{\varepsilon}_k^{(j)}|\boldsymbol{\gamma}^{(j)})$ using (11);
10  Compute the fault-condition probability $P(\boldsymbol{\gamma}^{(j)})$ with (13);
11  `den` $\leftarrow$ `den` $+ p(\boldsymbol{\varepsilon}_k^{(j)}|\boldsymbol{\gamma}^{(j)})P(\boldsymbol{\gamma}^{(j)})$;
12  **end**
13  $\hat{\boldsymbol{x}}_{k|k} \leftarrow \boldsymbol{0}$;
14  $\boldsymbol{T}_1, \boldsymbol{T}_2 \leftarrow \boldsymbol{0}$;
15  **for** $j = 1$ **to** $2^m - 1$ **do**
16  Compute the merging weight: $\xi^{(j)} \leftarrow p(\boldsymbol{\varepsilon}_k^{(j)}|\boldsymbol{\gamma}^{(j)})P(\boldsymbol{\gamma}^{(j)})/$`den`;
17  $\hat{\boldsymbol{x}}_{k|k} \leftarrow \hat{\boldsymbol{x}}_{k|k} + \xi^{(j)}\hat{\boldsymbol{x}}_{k|k}^{(j)}$;
18  $\boldsymbol{T}_1 \leftarrow \boldsymbol{T}_1 + \xi^{(j)}\boldsymbol{P}_{k|k}^{(j)}$;
19  **end**
20  **if** $\|\hat{\boldsymbol{x}}_{k|k} - \hat{\boldsymbol{x}}_{k-1|k-1}\|_2 > \bar{\Delta}$ **then**
21  $\hat{\boldsymbol{x}}_{k|k} \leftarrow \hat{\boldsymbol{x}}_{k|k-1}$;
22  $\boldsymbol{P}_{k|k} \leftarrow \boldsymbol{P}_{k|k-1}$;
23  **Continue**;
24  **end**
25  **for** $j = 1$ **to** $2^m - 1$ **do**
26  $\boldsymbol{T}_2 \leftarrow \boldsymbol{T}_2 + \xi^{(j)}\left(\hat{\boldsymbol{x}}_{k|k}^{(j)} - \hat{\boldsymbol{x}}_{k|k}\right)\left(\hat{\boldsymbol{x}}_{k|k}^{(j)} - \hat{\boldsymbol{x}}_{k|k}\right)^T$;
27  **end**
28  $\boldsymbol{P}_{k|k} \leftarrow \boldsymbol{T}_1 + \boldsymbol{T}_2$;
29 **end**

**TABLE 1. Noises levels used in the simulation.**

| Noise sources | Standard deviation (Dimensionless) |
|---|---|
| Process noise | 0.01 |
| LPC & HPC measurement noise | 0.001 |
| Generator-inferred HPC speed noise | 0.001 |
| Bleed-inferred HPC speed noise | 0.05 |

## IV. SIMULATION

### A. SIMULATION SETTINGS

To test the proposed method in estimating the spool rotation speeds of jet engines, we adopt a two-spool engine's (Tumansky R11-F300) linearized model given in [24]. The state of the system include the LPC and HPC speeds. The inputs are the fuel flow rate and exhaust nozzle area. The outputs include the directly measured LPC/HPC speeds, and the HPC speed inferred by the generator and bleed data.

The states, inputs and outputs are all dimensionless: Each variable is defined as the ratio of a physical value to its designed upper limit: E.g., the dimensionless HPC speed is represented as the ratio of the current HPC speed to the maximum HPC speed of the engine.

The sampling period of the simulation is 10 ms. Without loss of generality, we assume that the HPC speed inference algorithm has been given by other external modules. The dimensionless model parameters are then given by:

$$\begin{aligned} \boldsymbol{A_d} &= \begin{bmatrix} 0.9683 & 0.0094 \\ 0.0124 & 0.9781 \end{bmatrix}, \\ \boldsymbol{B_d} &= \begin{bmatrix} 0.0112 & 0.0188 \\ 0.0091 & 0.0001 \end{bmatrix}, \\ \boldsymbol{C_d} &= \begin{bmatrix} 1 & 0 \\ 0 & 1 \\ 0 & 1 \\ 0 & 1 \end{bmatrix}, \end{aligned} \tag{19}$$

where the first two rows of $\boldsymbol{C_d}$ correspond to the directly measured LPC and HPC speeds via the EIU, and the last two rows correspond to the generator and bleed-inferred HPC speeds shown in Fig. 1. Note that with the parameters in (19), it can be evaluated that the system is observable, as long as any one of the four output channels is working normally. This redundancy in measurements enables the use of state estimators, even if a subset of sensors are permanently malfunctioned (which will be demonstrated later).

Both the process and output noises are assumed to be zero-mean Gaussian noises. Stand deviations of the process and outputs noises are listed in Table 1. Note that the noise level of the bleed-inferred HPC speed is significantly larger than others, corresponding to a very inaccurate bleed-inference model. The covariances for the process noise ($\boldsymbol{Q}$) and output's noise $\boldsymbol{R}$ are assigned accordingly.

To emulate the smooth changes in the inputs (fuel flow rate and nozzle area), they were randomly generated using sums of sinusoidal signals with different frequencies, amplitudes, and phases. The simulation time is 10 s. The generated inputs for simulation are shown in Fig. 3.

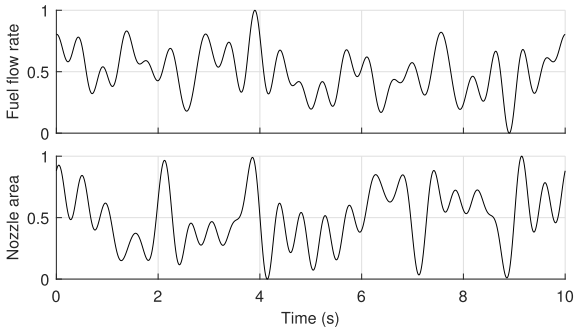


**FIGURE 3. Inputs of the two-spool jet engine in simulation.**

**TABLE 2. Fault conditions of the outputs in the simulation.**

| Outputs | Real $\boldsymbol{\lambda}$ | Guessed $\boldsymbol{\lambda}$ |
|---|---|---|
| LPC speed sensor | 0.80 | 0.90 |
| HPC speed sensor | 0.80 | 0.90 |
| Generator-inferred HPC speed | 0.90 | 0.95 |
| Bleed-inferred HPC speed | 0.97 | 0.95 |

The fault-condition parameters are given in Table 2. To make the simulations realistic, the following settings on sensor faults are made:

- Sensor faults randomly occur, following the fault-free probabilities given in Table 2 (real $\boldsymbol{\lambda}$). The faults exhibited intermittent behaviors, represented by the "spikes" in Fig. 4;
- Each faulty sensor's output at moment $k$ is a random number, uniformly distributed between 0 and 1;
- After 5 s, the first and second outputs are permanently malfunctioned, emulating a broken connection between the EIU and the EWD (Fig. 1). The resultant outputs are shown in Fig. 4;
- Despite the permanent faults and the real $\boldsymbol{\lambda}$ in Table 2, the expected $\boldsymbol{\lambda}$ implemented in (13) is a rough guess (third column of Table 2), which is a common situation in real practice.

The initial engine state is assumed to be $\boldsymbol{x}_0 = [0.30, 0.30]^T$, emulating the spools' idling speeds. The initial estimation is assumed to be $\hat{\boldsymbol{x}}_{0|0} = [0.28, 0.28]^T$, and $\boldsymbol{P}_{0|0} = \boldsymbol{Q}$. The variation threshold $\Delta$ (line 20 of Algorithm 1) is set to 0.05, meaning that a spool's speed cannot vary over 500% within 1 s, which is a very relaxed variation-rate limit. To quantify the estimation covariance $\boldsymbol{P}_{k|k}$ with a scalar, we define the *expected standard deviation percentage* as

$$\delta_{\text{exp}} = \sqrt{\text{trace}(\boldsymbol{P}_{k|k})/2} \times 100. \tag{20}$$

### B. SIMULATION RESULTS

Simulation results under the above settings are shown in Fig. 5, where the real system states, estimations, and the expected standard deviation percentage $\delta_{\text{exp}}$ are illustrated. According to Fig. 5, we can see that both the LPC and HPC speeds have been estimated successfully, despite the poor qualities of the sensors' feedbacks. Besides, the estimation covariance, quantified by the expected standard deviation percentage $\delta_{\text{exp}}$, has a significant increase after 5 s. This

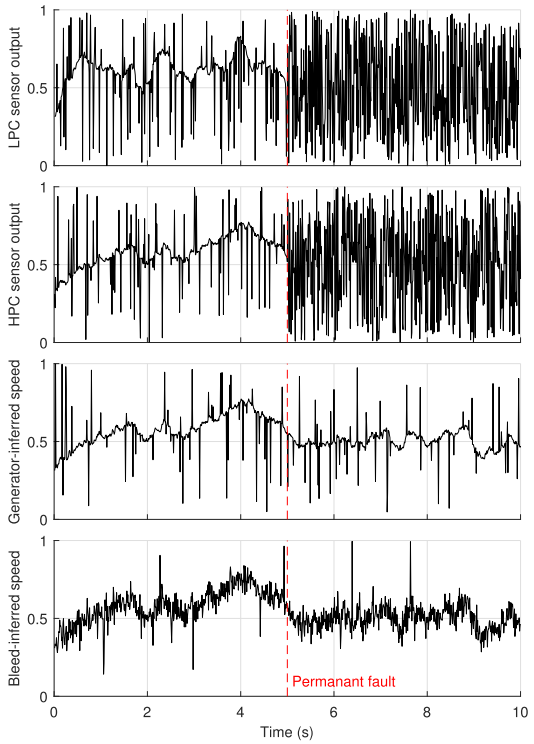


**FIGURE 4.** Sensor outputs under noises and temporary/permanent faults. The vertical dashed lines indicate the moment from which the first two sensors become permanently malfunctioned. The "spikes" in the outputs correspond to the intermittent sensor faults.

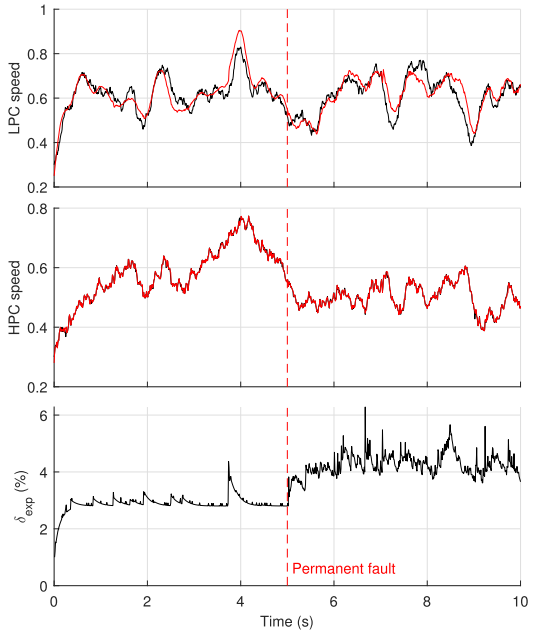


**FIGURE 5.** State estimation results using the proposed method. In the first and second rows, the black and red curves indicate the real and estimated spool speeds, respectively. The third row shows the expected standard deviation percentage given in (20). The vertical dashed lines indicate the moment from which LPC and HPC sensors become permanently malfunctioned.

increase in uncertainty is caused by the permanent faults in the first and second output channels.

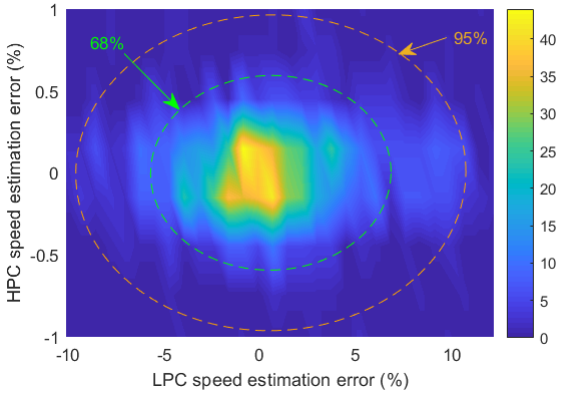


**FIGURE 6.** Histogram of the estimation errors. The green and orange ovals correspond to the 68% and 95% confidence ellipses.

On computational costs, a benchmark shows that the proposed method takes 578 floating point operations (FLOP) per iteration, and occupies 164 kB memory, which are compact enough for most embedded platforms. Besides, the computation time of the proposed algorithm in each iteration is approximately 0.5 ms, which is much smaller than the 10 ms sampling period, and is suitable for real-time applications.

To visualize the estimation errors defined as $\hat{\boldsymbol{x}}_{k|k} - \boldsymbol{x}_k$, a density plot is given in Fig. 6, showing the histogram and confidence ellipses of the estimation errors. According to the result, for the LPC speed estimation, we have 68% and 95% probabilities to achieve errors less than 6% and 11%, respectively. For the HPC speed estimation, we have 68% and 95% probabilities to achieve errors less than 0.6% and 1%, respectively. The relatively larger error in the LPC speed estimation is due to the fact that the LPC has only one direct measurement path, which is also more problematic than the HPC's measurement paths. Despite the difference between the LPC's and HPC's estimation errors, the demonstrated accuracies are still satisfactory for applications in human–machine interface.

### C. COMPARISON WITH OTHER METHODS

As some classic methods discussed in Section I are inapplicable to time-varying and intermittent faults, we have developed their modified versions for comparisons. The methods include:

1) Conditional correction using the classic KF (hereafter referred to as the classic KF correction): This corresponds to replacing the corrections in (7) and (8) (line 7 in Algorithm 1) using the classic KF, with the malfunctioned output paths removed for each fault condition. This method can be considered as an extended MMAE for time-varying fault conditions;
2) Fault detection using the $\chi^2$ test on the innovation errors within a time window (hereafter referred to as the $\chi^2$-based fault detection): This method keeps a record of the fault-free sensors' innovation errors, and performs $\chi^2$ test to check whether the current measurement data violates the Gaussian-distribution assump-

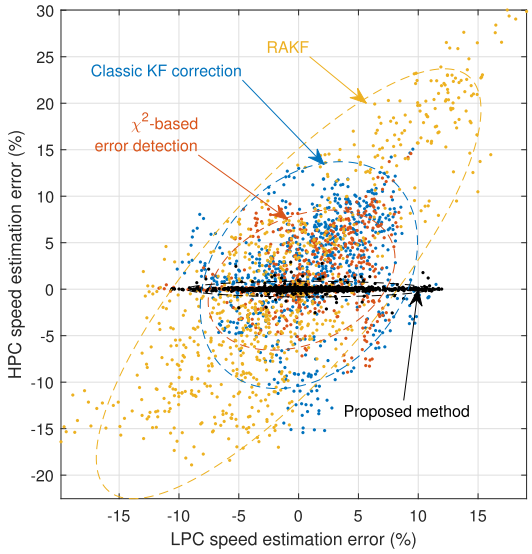


**FIGURE 7.** Scatter plot of the estimation errors. The blue, red, yellow, and black dots are the estimation errors corresponding to the classic-KF, $\chi^2$-based, RAKF, and the proposed methods, respectively. The dashed ellipses show the errors' distribution regions of the four methods with 95% confidence.

**TABLE 3.** Comparing the estimation errors of four estimation methods.

| Methods | $\|\text{mean}(\hat{\boldsymbol{x}} - \boldsymbol{x})\|_2$ (%) | Ellipse area $a_{95\%}$ |
|---|---|---|
| RAKF | 1.02 | 685.80 |
| classic KF correction | 1.73 | 332.87 |
| $\chi^2$-based fault detection | 1.01 | 175.58 |
| Proposed method | 0.77 | 26.79 |

tion. In the simulation, the length of the time window is set to 100, and the $\alpha$ value of the $\chi^2$ test is set to 0.05. This method can be considered as an extended IAE for intermittent measurements;

3) Robust adaptive KF (RAKF): An instantaneous $\chi^2$-threshold-based method is used to detect faults in real time. The estimation process is based on classic KF, whereas an adaption rule on the covariance matrix $\boldsymbol{R}$ is invoked when a fault is detected. The adaption needs a record of innovation errors within a time window. In the simulation, the window length is 200, and the $\alpha$ value for $\chi^2$ test is set to 0.01—Both the window length and the $\alpha$ value are tuned by a trial-and-error process.

With the above methods, simulations are performed with the same inputs, fault conditions, and sensor outputs. The resultant estimation errors are compared with those of the proposed method in Fig. 7. Comparing the sizes of the error distribution regions and the confidence ellipses, we can see that the proposed method leads to the significantly reduced estimation errors.

Another set of results are given in Table 3, where the areas of the 95%-confidence ellipses, denoted by $a_{95\%}$, are adopted for comparing different methods. According to the comparisons in Fig. 7 and Table 3, we can see that

- RAKF does not perform well in the simulation. Though being the state-of-the-art method [12], it is not designed to address intermittent faults, as adaption is not sufficiently fast to catch up with the instantaneously-varying fault conditions;
- For the classic KF correction, though the malfunctioned sensor paths are removed, the estimation accuracy is still not as good as the IMKF, which is optimized for intermittent faults;
- The $\chi^2$-based fault detection relies on the normality test of the innovation errors in the time window; a temporary error is not significant enough to trigger a non-Gaussian (i.e., fault) judgement. This result emphasizes the importance of the conditional correction and merging steps in Section III.

Comparing with the RAKF, classic-KF-based and $\chi^2$-based methods, the proposed method results in approximately 24%, 55%, and 24% reductions in the mean errors, and 96%, 92%, and 85% reductions in the distribution areas, which support the effectiveness of the proposed method.

**TABLE 4.** Effects of noise types on estimation errors.

| Noise types | $\|\text{mean}(\hat{\boldsymbol{x}} - \boldsymbol{x})\|_2$ (%) | Ellipse area $a_{95\%}$ |
|---|---|---|
| Gaussian | 0.77 | 26.79 |
| Laplace | 0.31 | 40.87 |
| Cauchy | 1.40 | 193.18 |

### D. EFFECTS OF NON-GAUSSIAN MEASUREMENT NOISES

In many cases, the measurement noises are non-Gaussian, and the optimality of KF is not preserved. For state-estimations under non-Gaussian and heavy-tailed noises, researchers have proposed many ad-hoc filters (e.g., [25]–[28]) and addressed their optimality issues (which are beyond our scope). In practice, however, the KF-based approaches are still widely adopted for simplicity. Therefore, in the simulation, we tested the performances of the proposed method under the following non-Gaussian noises:

- Zero-mean Laplace noises with standard deviations of $7.50 \times 10^{-4}$ (for the first three output channels) and $3.75 \times 10^{-2}$ (for the last output channel);
- Zero-mean Cauchy noises with one degree of freedom, and scale parameters as $2.38 \times 10^{-4}$ (for the first three output channels) and $1.19 \times 10^{-2}$ (for the last output channel).

The above parameters are chosen to keep the 95% measurement errors within the $\pm 0.003$ (for the first three output channels) and $\pm 0.15$ (for the last output channel) limits, whereas for the same limits, the Gaussian noises in Table 1 have 99.7% confidence. With the above noise types, simulations are performed with the proposed method. The effects of non-Gaussian noises on the estimation errors are shown in Fig. 8, and the error comparison under different noises is listed in Table 4.

According to the results in Fig. 8 and Table 4, the introduction of Laplace noises leads to slight accuracy decrease, whereas the Cauchy noises correspond to significantly larger

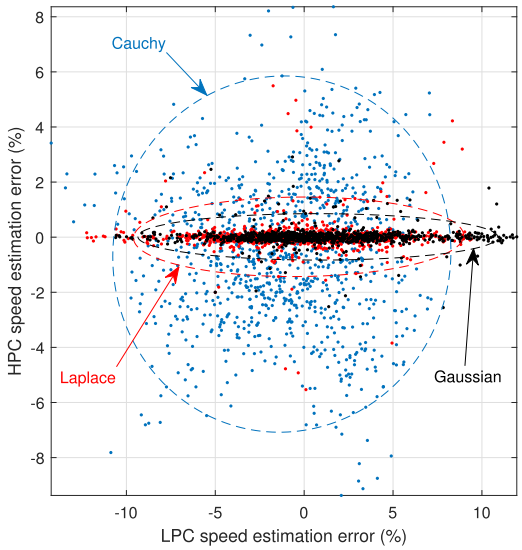


**FIGURE 8.** Scatter plot of the estimation errors under different types of measurement noises. The blue, red, and black dots are the estimation errors corresponding to the Cauchy, Laplace, and Gaussian noises, respectively. The dashed ellipses show the error-distribution regions with 95% confidence.

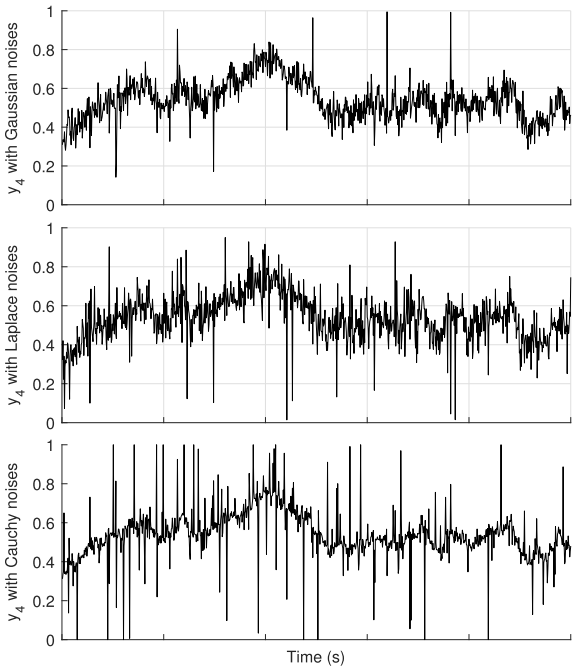


**FIGURE 9.** Comparison of the fourth channel's outputs under different types of noises.

estimation errors. This is because the Cauchy noises include much more extremal measurement errors — this can be seen in Fig. 9, whose bottom row (i.e., the fourth output channel under the Cauchy noise) have significantly more "spikes" than the first two rows. On the other hand, these largely-deviated errors are equivalent to intermittent sensor faults, hence can be automatically handled by the proposed method. As a result, the estimation performance under the Cauchy noises is still comparable to that of the $\chi^2$-based method under the Gaussian noises.

## V. CONCLUSION

Achieving analytical redundancy without additional hardware is an attractive way of enhancing aviation safety, whereas state estimation under diversified sensor faults is non-trivial. In this paper, to realize robust state estimation under unknown, time-varying and featureless sensor faults, we propose a new state estimation method based on the intermittent-measurement Kalman filter and the Bayesian-probability-weighted Gaussian mixture reduction. The formulated method is implemented in an application of monitoring a jet engine's spool speeds. Simulation results show that the proposed method leads to the significantly enhanced robustness and accuracy in state estimations.

To improve the present work, the proposed method is to be extended to a nonlinear version by combining it with the extended or unscented Kalman filters. Besides, special versions of the filters should be considered to deal with various types of non-Gaussian noises. Finally, compared with the quadratic objective function in the Kalman filter, the weighted absolute value [29] and maximum exponential absolute value [30] provides intrinsic robustness to bad measurements and may lead to improved FDI/estimation performance. These issues are to be explored in the future work.

## REFERENCES

[1] F. Amato, C. Cosentino, M. Mattei, and G. Paviglianiti, "A direct/functional redundancy scheme for fault detection and isolation on an aircraft," *Aerosp. Sci. Technol.*, vol. 10, no. 4, pp. 338–345, May 2006.

[2] AMETEK. *Datasheet of Engine Interface Unit*. Accessed: Dec. 2019. [Online]. Available: http://www.ametekpds.com/products/data-acquisition-units/engine-interface-unit

[3] F. A. Administration. *FAA Advisory Circular 33.28-1: Aircraft Engines, Electrical and Electronic Engine Control Systems*. Accessed: Jun. 2006. [Online]. Available: https://go.usa.gov/xn89k

[4] R. J. Patton, "Fault detection and diagnosis in aerospace systems using analytical redundancy," *Comput. Control Eng. J.*, vol. 2, no. 3, pp. 127–136, May 1991.

[5] R. J. Patton and J. Chen, "Robust fault detection of jet engine sensor systems using eigenstructure assignment," *J. Guid., Control, Dyn.*, vol. 15, no. 6, pp. 1491–1497, Nov. 1992.

[6] D. Magill, "Optimal adaptive estimation of sampled stochastic processes," *IEEE Trans. Autom. Control*, vol. AC-10, no. 4, pp. 434–439, Oct. 1965.

[7] R. A. Gray and P. S. Maybeck, "An integrated GPS/INS/baro and radar altimeter system for aircraft precision approach landings," in *Proc. IEEE Nat. Aerosp. Electron. Conf. (NAECON)*, vol. 1, May 1995, pp. 161–168.

[8] Y. Zhang and X. R. Li, "Detection and diagnosis of sensor and actuator failures using IMM estimator," *IEEE Trans. Aerosp. Electron. Syst.*, vol. 34, no. 4, pp. 1293–1313, Oct. 1998.

[9] P. S. Maybeck, "Multiple model adaptive algorithms for detecting and compensating sensor and actuator/surface failures in aircraft flight control systems," *Int. J. Robust Nonlinear Control*, vol. 9, no. 14, pp. 1051–1070, Dec. 1999.

[10] C. D. Ormsby, J. F. Raquet, and P. S. Maybeck, "A new generalized residual multiple model adaptive estimator of parameters and states," *Math. Comput. Model.*, vol. 43, nos. 9–10, pp. 1092–1113, May 2006.

[11] C. Hajiyev and F. Caliskan, "Sensor/actuator fault diagnosis based on statistical analysis of innovation sequence and robust Kalman filtering," *Aerosp. Sci. Technol.*, vol. 4, no. 6, pp. 415–422, Sep. 2000.

[12] C. Hajiyev and H. E. Soken, "Robust adaptive Kalman filter for estimation of UAV dynamics in the presence of sensor/actuator faults," *Aerosp. Sci. Technol.*, vol. 28, no. 1, pp. 376–383, Jul. 2013.

[13] P. Lu, L. Van Eykeren, E.-J. Van Kampen, Q. P. Chu, and B. Yu, "Adaptive hybrid unscented Kalman filter for aircraft sensor fault detection, isolation and reconstruction," in *Proc. AIAA Guid., Navigat., Control Conf.*, Jan. 2014, p. 1145.

[14] S. J. Julier and J. K. Uhlmann, "Unscented filtering and nonlinear estimation," *Proc. IEEE*, vol. 92, no. 3, pp. 401–422, Mar. 2004.
[15] R. Mehra, "On the identification of variances and adaptive Kalman filtering," *IEEE Trans. Autom. Control*, vol. AC-15, no. 2, pp. 175–184, Apr. 1970.
[16] R. Mehra, "On-line identification of linear dynamic systems with applications to Kalman filtering," *IEEE Trans. Autom. Control*, vol. AC-16, no. 1, pp. 12–21, Feb. 1971.
[17] T. Kailath, "A note on least-squares estimation by the innovations method," in *Proc. IEEE Conf. Decis. Control*, Dec. 1971, pp. 407–411.
[18] A. H. Mohamed and K. P. Schwarz, "Adaptive Kalman filtering for INS/GPS," *J. Geodesy*, vol. 73, no. 4, pp. 193–203, May 1999.
[19] B. Sinopoli, L. Schenato, M. Franceschetti, K. Poolla, M. I. Jordan, and S. S. Sastry, "Kalman filtering with intermittent observations," *IEEE Trans. Autom. Control*, vol. 49, no. 9, pp. 1453–1464, Sep. 2004.
[20] C. Yang, J. Zheng, X. Ren, W. Yang, H. Shi, and L. Shi, "Multi-sensor Kalman filtering with intermittent measurements," *IEEE Trans. Autom. Control*, vol. 63, no. 3, pp. 797–804, Mar. 2018.
[21] R. Prakash, S. V. Rao, and C. A. Skarvan, "Life enhancement of a gas turbine engine by temperature control," *Int. J. Turbo Jet Engines*, vol. 7, nos. 3–4, Jan. 1990.
[22] A. R. Runnalls, "Kullback-leibler approach to Gaussian mixture reduction," *IEEE Trans. Aerosp. Electron. Syst.*, vol. 43, no. 3, pp. 989–999, Jul. 2007.
[23] M. R. Rajamani and J. B. Rawlings, "Estimation of the disturbance structure from data using semidefinite programming and optimal weighting," *Automatica*, vol. 45, no. 1, pp. 142–148, Jan. 2009.
[24] R. Lungu, A. N. Tudosie, and L. Dinca, "Double-Spool Single Jet Engine for Aircraft as Controlled Object," *Int. J. Math. Models Methods Appl. Sci.*, vol. 2, no. 4, pp. 553–562, 2008.
[25] C. Masreliez, "Approximate non-Gaussian filtering with linear state and observation relations," *IEEE Trans. Autom. Control*, vol. AC-20, no. 1, pp. 107–110, Feb. 1975.
[26] E. Daeipour and Y. Bar-Shalom, "An interacting multiple model approach for target tracking with glint noise," *IEEE Trans. Aerosp. Electron. Syst.*, vol. 31, no. 2, pp. 706–715, Apr. 1995.
[27] W. Niehsen, "Robust Kalman filtering with generalized Gaussian measurement noise," *IEEE Trans. Aerosp. Electron. Syst.*, vol. 38, no. 4, pp. 1409–1412, Oct. 2002.
[28] M. Roth, E. Ozkan, and F. Gustafsson, "A Student's t filter for heavy tailed process and measurement noise," in *Proc. IEEE Int. Conf. Acoust., Speech Signal Process.*, May 2013, pp. 5770–5774.
[29] Y. Chen, F. Liu, S. Mei, and J. Ma, "A robust WLAV state estimation using optimal transformations," *IEEE Trans. Power Syst.*, vol. 30, no. 4, pp. 2190–2191, Jul. 2015.
[30] Y. Chen, J. Ma, P. Zhang, F. Liu, and S. Mei, "Robust state estimator based on maximum exponential absolute value," *IEEE Trans. Smart Grid*, vol. 8, no. 4, pp. 1537–1544, Jul. 2017.

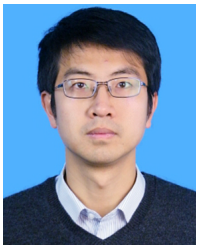

**HONGBO WANG** (Member, IEEE) received the B.S. and M.S. degrees in mechanical engineering from Tsinghua University, Beijing, China, in 2006 and 2009, respectively, and the Ph.D. degree in bioengineering and robotics from Tohoku University, Sendai, Japan, in 2012.

From 2012 to 2015, he was a Research Assistant with the Department of Bioengineering and Robotics, Tohoku University. He is currently an Associate Professor with the School of Mechanical Engineering, Northwestern Polytechnical University, Xi'an, China. His research interests include robust control and aircraft prognostics.

**DONG LIU** received the B.S. and M.S. degrees in electronics and information engineering from the Nanjing University of Aeronautics and Astronautics, Nanjing, China, in 2006 and 2009, respectively.

He is currently a Chief Designer of aircraft vehicle system with the First Aircraft Institute, Aviation Industry Corporation of China (AVIC). His research interests include aircraft prognostics and health management, avionics software, and system engineering.

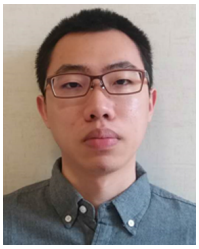

**TIANYU CHEN** is currently pursuing the bachelor's degree with the School of Electronic Engineering, Xi'an University of Posts and Telecommunications, China. He is also an Intern with the First Aircraft Institute, Aviation Industry Corporation of China. His research interest includes aircraft prognostics and health management.

**XIANSHENG QIN** (Member, IEEE) received the B.S., M.S., and Ph.D. degrees in aerospace manufacturing engineering from Northwestern Polytechnical University (NPU), Xi'an, China, in 1983, 1986, and 1991, respectively.

He is currently a Professor with the School of Mechanical Engineering, NPU. He is also the Director of the NPU–Xi'an Aircraft Corporation Center of Aviation Manufacturing Systems. For over three decades, he has been focused on solving the real-world problems in aerospace manufacturing, mechatronics, and system engineering. He received the AVIC Science Progress Award from the Aviation Industry Corporation of China, in 1998, and the Rong Hong Award from the United Technologies (now Raytheon Technologies), in 1999.